Predicted structure and stability of $A_4B_3O_{12}$ δ-phase compositions

C. R. Stanek,* C. Jiang, B. P. Uberuaga, and K. E. Sickafus
Materials Science and Technology Division, Los Alamos National Laboratory, Los Alamos, New Mexico 87545, USA

A. R. Cleave and R. W. Grimes
Department of Materials, Imperial College London, London SW7 2BP, United Kingdom
(Received 4 May 2009; revised manuscript received 29 July 2009; published 2 November 2009)

A combination of atomistic simulation techniques has been employed to predict ordered structures for a series of $A_4B_3O_{12}$ δ-phase compounds, where A is a 3+ cation ranging in size from Sc^{3+} to Ho^{3+} and B is a 4+ cation ranging from Ti^{4+} to Zr^{4+}. Experimentally, a fully ordered cation structure has yet to be resolved for any of these compounds. Monte Carlo energy-minimization calculations using short-range pair potentials identified three low-energy arrangements of A^{3+} and B^{4+} cations. The details of these three structures were analyzed with the layer motif method. To quantitatively determine the δ-phase structure of each composition, the three configurations were reevaluated with density-functional theory. We also used special quasirandom structures to compare the ordered low-energy configurations to cation disorder. For all compositions considered, we find that at least one of the three ordered structures is lower in energy than the disordered structure, suggesting the thermodynamic stability of an ordered phase. Of the three ordered structures identified by this approach, one has not been identified previously in the literature for any composition. In addition, we discuss the stability of δ-phase compounds with respect to other "ABO_{4-x}" fluorite-derivative compositions and predict the structure of compositions for which none has been reported.

DOI: 10.1103/PhysRevB.80.174101 PACS number(s): 61.50.Ah, 61.66.Fn, 61.72.−y, 71.15.Mb

I. INTRODUCTION

Oxide materials crystallizing with the fluorite structure or derivatives of the fluorite structure (i.e., related to the mineral *fluorite* CaF_2) exhibit a variety of materials properties that make fluorites suitable for a wide range of technological applications including thermal barrier coatings,[1] electrolytes in solid oxide fuel cells,[2–4] nuclear fuel,[5,6] and crystalline nuclear waste forms.[7,8] When contemplating the selection of a fluorite-derivative material for a specific application, it is important to understand how the materials properties of complex oxides (i.e., with more than one cation sublattice, such as $A_2B_2O_7$ pyrochlore) may vary within a subfamily, as a function of composition. For example, it has been found that certain $A_2Zr_2O_7$ zirconate pyrochlores (e.g., $Er_2Zr_2O_7$) maintain crystallinity during exposure to ion irradiation,[8,9] which is a behavior similar to cubic ZrO_2—a prototypic fluorite oxide.[10] Conversely, all $A_2Ti_2O_7$ titanate pyrochlore compounds are susceptible to amorphization under similar intense irradiation conditions.[8,9] This example demonstrates that for "ABO_{4-x}" fluorite derivatives (where this chemical formula actually represents compounds of the cumbersome formula $A_m^{3+}B_n^{4+}O_{3m/2+2n}$, with $m \approx n$), simple alterations of the chemistry may significantly alter the structure-property relations. It follows that improved understanding of the effects of compositional variation will lead to enhanced control of the materials properties of fluorite-related materials.

As Kurnakov suggested nearly 100 years ago,[11] it is worthwhile to establish trends in the properties of solids as a function of compositional variation ("physicochemical analysis," according to Kurnakov). Specifically for radiation tolerance, we have previously attempted to relate the resistance to amorphization under irradiation of $A_2B_2O_7$ pyrochlores and related disordered fluorite compounds to the composition of the compound.[8] From our studies, we have found that compounds with a natural tendency to accommodate lattice disorder are those that exhibit the best amorphization resistance characteristics.[8,12] By using this criterion, we have recently identified another family of radiation tolerant fluorite-derivative compounds—the so-called δ-phase oxides of the type $A_4B_3O_{12}$.[13] For these compounds, A is a 3+ cation ranging in ionic size from Sc^{3+} (0.87 Å) to Ho^{3+} (1.015 Å) and B is a 4+ cation ranging from Ti^{4+} (0.74 Å) to Zr^{4+} (0.72 Å).[14] However, the description of the δ-phase structure is incomplete across this entire compositional range. Only after developing a complete understanding of the δ-phase structure will it be appropriate to commence a systematic comparison of its structure-property relations with those of other fluorite derivatives. The unresolved issue for the δ-phase structure is the arrangement of A^{3+} and B^{4+} cations; a fully ordered arrangement of cations has not been observed after a number of experimental studies.[15–22] Apart from the cation ordering, the δ-phase structure is understood as a defect fluorite with ordered structural oxygen vacancies (that is, unoccupied crystallographic symmetry sites) along $\langle 111 \rangle$. There are two cation sites, 3*a* and 18*f* in Wyckoff notation. For A^{3+} and B^{4+} cations with dissimilar radii, e.g., Sc^{3+} and Sn^{4+},[21] the B cation is said to exclusively occupy the 3*a* site, which accounts for 1/7 of all cation sites and is sixfold coordinated by oxygen. The remaining cations reside on the 18*f* site and there is no experimental evidence of further ordering on this site. It has been proposed intuitively that compounds with similar radii will show less cation ordering than those of dissimilar radii.[21]

Two previous papers, both by Bogicevic *et al.*, have used density-functional theory (DFT) to predict ordered cation structures of two δ-phase compounds: $Y_4Zr_3O_{12}$ (Ref. 23) and $Sc_4Zr_3O_{12}$.[24] In the first of these papers, a cation arrangement for $Y_4Zr_3O_{12}$ was predicted by calculating the lattice

energy for 45 different configurations of a 19-atom cell. The 45 configurations were determined by a lattice algebra technique, which was originally used to determine the structure of κ-Al_2O_3.[25] For the ordered structure of $Y_4Zr_3O_{12}$, Bogicevic *et al.*[23] predicted the $3a$ sites to be exclusively occupied by Zr^{4+} and the $18f$ sites occupied by Y^{3+} and Zr^{4+} in an ordered arrangement. This result was confirmed in a recent theoretical study by Predrith, *et al.*[26] A separate but similar study by Bogicevic *et al.*[24] revealed a different δ-phase structure for $Sc_4Zr_3O_{12}$. In this structure, the sixfold $3a$ site was occupied by Sc^{3+} rather than Zr^{4+}, although the cations were still ordered.

In this paper, we predict the structures of 17 $A_4B_3O_{12}$ δ-phase compounds (including $Y_4Zr_3O_{12}$ and $Sc_4Zr_3O_{12}$) and in the process introduce a heretofore unobserved cation arrangement. To minimize the number of computationally intensive DFT calculations and to allow for the consideration of large simulation cells, we have used a self-consistent set of pair potentials to perform Monte Carlo simulations that efficiently identify low-energy cation arrangements. These low-energy structures were subsequently examined with DFT for higher fidelity quantification of structural stability. Finally, we used special quasirandom structures (SQS) (Refs. 27–29) to compare our ordered structures to disordered structures. Details of these methods are provided in the following sections.

II. METHODOLOGY

A. Pair-potential energy-minimization simulations

The empirical calculations presented here are based upon a classical Born-type description of an ionic crystal lattice.[30] The crystal is composed of an infinite array of isotropic spherical point charges. Forces acting between ions are resolved into two terms: long-range Coulombic forces, summed using the Ewald method,[31] and isotropic short-range forces, which are modeled using parametrized pair potentials. The perfect lattice is defined by a unit cell, which is effectively repeated through all space using periodic boundary conditions. The lattice energy, $E(r_{ij})$, can then be expressed as

$$E = \frac{1}{2}\sum_{i}^{n}\sum_{j\neq i}^{n}\left[\frac{q_i q_j}{4\pi\epsilon_o r_{ij}} + A_{ij}\exp\left(-\frac{r_{ij}}{\rho_{ij}}\right) - \frac{C_{ij}}{r_{ij}^6}\right], \quad (1)$$

where A, ρ, and C are potential parameters of the Buckingham type[32] specific to the pair of ions i and j, r_{ij} is the interionic separation, and q_i is the charge of ion i. The parameters employed were self-consistently derived specifically for the δ-phase structure and are given in Table I. All ions were considered with partial charges as follows: $A^{3+}=2.55$, $B^{4+}=3.4$, and $O^{2-}=-1.7$. Additional details of this computational method can be found elsewhere.[33]

B. Combined energy minimization—Monte Carlo (CEMMC)

A comprehensive study of cation disorder in δ-phase compounds is problematic; even within a single unit cell there are many possible configurations of the cation sublattice. The CEMMC technique allows us to sample the possible degrees of disorder through configurational averaging. It has been demonstrated previously that this technique can describe Al-Fe disorder involving uncharged defects in $Ca_2Fe_xAl_{2-x}O_5$ brownmillerite, over the entire compositional range $(0\leq x\leq 2.0)$,[34,35] and Al-Mg disorder involving charged defects in a study of cation antisite disorder of $MgAl_2O_4$ spinel.[36] Here, energy minimization using the self-consistent short-range pair potentials described in the previous section was used to obtain the energy and lattice properties for multiple arrangements of A^{3+} and B^{4+} within a periodically repeated hexagonal cell of stoichiometric $A_4B_3O_{12}$ (which contains 54 ions). The arrangements are generated using the Metropolis statistical sampling Monte Carlo technique[37] as follows. At a given iteration, the system has the cation configuration μ of energy E_μ. Two randomly chosen cations are then exchanged, forming a new configuration υ. The lattice is reminimized and the new energy, E_υ, is calculated and the new configuration is adopted in place of the old with probability W,

$$W_{\mu\rightarrow\upsilon} = \begin{cases} \exp\dfrac{-\Delta E}{kT}, & \Delta E > 0 \\ 1, & \Delta E < 0 \end{cases}, \quad (2)$$

where T is the target temperature, k is Boltzmann's constant and $\Delta E = E_\upsilon - E_\mu$. In order to generate different overall de-

TABLE I. Buckingham pair-potential parameters.

Ions (i-j)	A_{ij} (eV)	ρ (Å)	C_{ij} (eV Å^6)
La^{3+}-O^{2-}	2306.26	0.3263	23.25
Pr^{3+}-O^{2-}	2236.02	0.3225	23.94
Nd^{3+}-O^{2-}	2205.88	0.3206	22.59
Sm^{3+}-O^{2-}	2179.20	0.3181	21.28
Eu^{3+}-O^{2-}	2172.45	0.3168	20.59
Gd^{3+}-O^{2-}	2165.40	0.3158	19.90
Tb^{3+}-O^{2-}	2137.47	0.3138	19.25
Dy^{3+}-O^{2-}	2130.65	0.3121	18.68
Y^{3+}-O^{2-}	2107.60	0.3109	17.51
Ho^{3+}-O^{2-}	2113.67	0.3110	18.16
Er^{3+}-O^{2-}	2103.60	0.3097	17.55
Yb^{3+}-O^{2-}	2075.26	0.3076	16.57
Lu^{3+}-O^{2-}	2069.99	0.3067	16.87
In^{3+}-O^{2-}	2001.65	0.3016	11.85
Sc^{4+}-O^{2-}	1944.21	0.2960	11.85
Ti^{4+}-O^{2-}	1865.80	0.2946	0.0
Ru^{4+}-O^{2-}	1883.39	0.2954	0.0
Mo^{4+}-O^{2-}	1901.50	0.3011	0.0
Sn^{4+}-O^{2-}	1945.41	0.3099	13.66
Hf^{4+}-O^{2-}	1951.95	0.3126	17.21
Zr^{4+}-O^{2-}	1953.80	0.3109	5.10
Pb^{4+}-O^{2-}	2005.10	0.3203	19.50
Ce^{4+}-O^{2-}	2058.36	0.3292	22.50
O^{2-}-O^{2-}	4870.00	0.2670	77.0

grees of disorder different target temperatures were employed (clearly a higher temperature gives rise to a greater overall degree of disorder). For each target temperature 10 000 swap attempts (as opposed to successful swaps) were made.

C. Density-functional theory

First-principles calculations were performed using the all-electron projector-augmented wave method[38] within the generalized gradient approximation of Perdew, Burke, and Ernzerhof (PBE-GGA),[39] as implemented in Vienna *ab initio* simulation package (VASP).[40–43] According to our convergence tests, a plane-wave cutoff energy of 400 eV and a $2\times2\times2$ k-point sampling are sufficient to give fully converged results. By computing the quantum-mechanical forces and stress tensor, the lattice parameters and internal atomic positions of all structures are fully optimized using a conjugate-gradient scheme. Although δ-phase compounds exist where the A^{3+} cation is Yb^{3+}, we were unable to obtain reliable results for this particular cation. The reason for this is that the PBE-GGA pseudopotentials for Eu and Yb are different than the other A cations. For cations between La and Lu, we employed charge-specific GGA pseudopotential, where some of the f electrons are kept frozen in the core. For all cations between La and Lu, except Eu and Yb, the charge-specific pseudopotential is trivalent. Previous studies have indicated that Eu and Yb exhibit a valence less than 3,[44] and previous DFT simulation studies have encountered similar convergence issues for Eu and Yb oxides (e.g., Ref. 45) Regardless, for this reason, we do not discuss $Yb_4B_3O_{12}$ compounds in Sec. III (and there are no δ-phase compounds for which the A cation is Eu).

In order to estimate the order-disorder energetics of $A_4B_3O_{12}$ δ phases, we have also considered a disordered version of the δ phase, in which the $3a$ sites are exclusively occupied by B^{4+} cations while the $18f$ sites are randomly occupied by both A^{3+} and B^{4+} cations. Clearly, this structure does not represent complete disorder and rather is more representative of experimentally observed structures [where, for all δ-phase compounds, the $3a$ is exclusively occupied by the B^{4+} cation, except for $Sc_4Zr_3O_{12}$, where the $3a$ site is randomly occupied by Sc^{3+} and Zr^{4+} (Refs. 15–22)]. The oxygen atoms remain fully ordered. We adopted the SQS approach[27–29] to adequately reproduce the statistics of a cation-disordered structure in a relatively small (thus computationally feasible) 57-atom periodic supercell. As will be shown, the total energy difference between the fully ordered ground-state δ-phase structure and the SQS is generally quite small, giving rise to a low order-disorder transition temperature.

III. RESULTS

A. ABO_{4-x} structural stability

To understand the compositional dependence on the structure of δ-phase compounds in relation to other fluorite derivatives, we have developed an "$A^{3+}B^{4+}O_{4-x}$" structure map of the type pioneered by Roy,[46] see Fig. 1. (Recall, this map

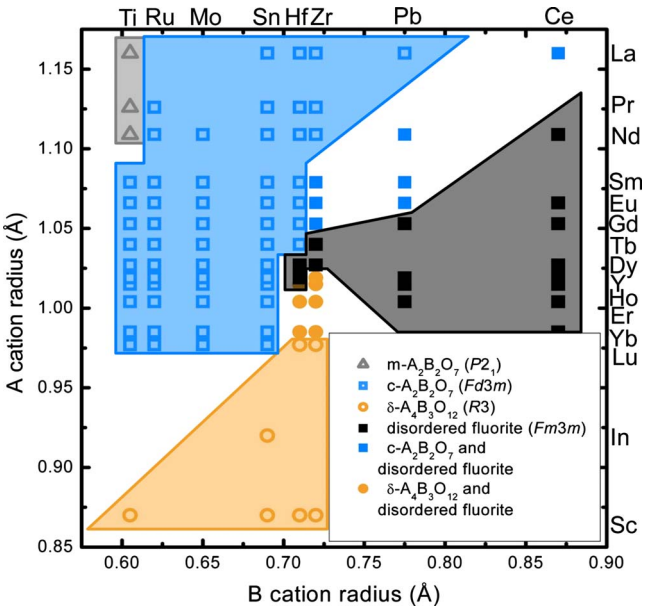

FIG. 1. (Color online) Structure map for $A^{3+}B^{4+}O_{4-x}$ compounds from reported structures. Hollow gray triangles denote the monoclinic $A_2B_2O_7$ structure (space group $P2_1$, No. 4) from Refs. 47–52, hollow blue squares denote $A_2B_2O_7$ pyrochlore (space group $Fd\bar{3}m$, No. 227) from Refs. 53–87, and hollow orange circles denote the rhombohedral $A_4B_3O_{12}$ δ phase (space group $R\bar{3}$, No. 148) from Refs. 15–22 and 88–91). Solid black squares denote disordered fluorite (space group $Fm\bar{3}m$, No. 225) from Refs. 92–107. Solid symbols of the same shape as stable ordered structures denote that both the ordered structure and disordered fluorite have been observed.

actually presents structures with the cumbersome formula $A_m^{3+}B_n^{4+}O_{3m/2+2n}$, where $m\approx n$). This structure map describes the experimentally observed crystal structure of oxygen-deficient fluorite compounds according to the cation radius of the constituent cations, where A is a eightfold-coordinated 3+ cation ranging from Sc^{3+} to La^{3+} and B is a sixfold-coordinated 4+ cation ranging from Ti^{4+} to Ce^{4+}. Not all of the structures considered in this map exhibit these exact cation coordinations (e.g., δ phase). Nevertheless, for structural trends, the map is instructive. In Fig. 1, combinations of A^{3+} and B^{4+} cations that form stable cubic pyrochlores, $A_2B_2O_7$, are denoted by hollow blue squares; $A_4B_3O_{12}$ δ-phase compounds are denoted by hollow orange circles; and monoclinic pyrochlores are denoted by hollow gray triangles. Disordered fluorites are denoted by solid black squares. Where both disordered fluorite and an ordered phase have been experimentally observed, a solid symbol corresponding to the ordered compound appears (e.g., solid blue squares denote both pyrochlore and disordered fluorite). It is evident from Fig. 1 that the δ-phase series of compounds exists within a triangular compositional range having vertices roughly at Sc^{3+}-Ti^{4+}, Sc^{3+}-Zr^{4+}, and Yb^{3+}-Zr^{4+}. In addition to the δ-phase compounds that fall within this compositional space (including stoichiometric compounds for which no experimental data exists, e.g., $In_4Zr_3O_{12}$), we also consider, in this paper, compositions for which both δ-phase and disordered fluorite structures have been observed (solid orange circles in Fig. 1).

Before we proceed with the discussion of our computational results, we are in a position to use Fig. 1 in combination with cationic radii[14] to revisit and update ionic radius-ratio factors for structural predictions (i.e., $r_{A^{3+}}/r_{B^{4+}}$, using eightfold and sixfold radii, respectively). Brisse and Knop[53] originally used the ionic radii of Pauling,[108] Ahrens,[109] and Templeton and Dauben[110] to develop radius ratios to indicate the stability limit of pyrochlore; they predicted the upper limit to be "at least" the value for $La_2Sn_2O_7$ ($r_{La^{3+}}/r_{Sn^{4+}}=1.68$ according to Shannon[14]), and the lower limit to be $Lu_2Sn_2O_7$ [$r_{Lu^{3+}}/r_{Sn^{4+}}=1.42$ (Ref. 14)].[53] Although $Lu_2Sn_2O_7$ remains a representative indicator of the lower bound of pyrochlore stability, $Sm_2Ti_2O_7$ is a stable pyrochlore and has a radius ratio larger than $La_2Sn_2O_7$ ($r_{Sm^{3+}}/r_{Ti^{4+}}=1.78$). Therefore, we can redefine the pyrochlore stability limits as $r_{A^{3+}}/r_{B^{4+}}$ between 1.42 and 1.78. Interestingly, we have previously predicted the possible formation of three pyrochlore compounds not observed experimentally but within this stability limit, namely, e.g., $Dy_2Hf_2O_7$, $Ho_2Hf_2O_7$,[111] and $Tb_2Zr_2O_7$.[112] Recent experiments preliminarily support the formation of $Dy_2Hf_2O_7$.[85] For $P2_1$ monoclinic pyrochlores, the lower limit is $Nd_2Ti_2O_7$ ($r_{Nd^{3+}}/r_{Ti^{4+}}=1.83$) and the upper limit is at least $La_2Ti_2O_7$ ($r_{La^{3+}}/r_{Ti^{4+}}=1.92$). Therefore, the radius ratio $r_{A^{3+}}/r_{B^{4+}}$ for the monoclinic $A_2B_2O_7$ phase field ranges from 1.83 to 1.92 (and possibly beyond), and the monoclinic to cubic pyrochlore boundary lies somewhere between 1.78 and 1.83. For δ phase, the stability limit appears to have a lower bound of $\approx$1.21 at $Sc_4Zr_3O_{12}$ and an upper bound at $Sc_4Ti_3O_{12}$ (1.44). The distinction between pyrochlore and δ phase is not sharp, which is commensurate with the controversy over the existence of $Y_2Zr_2O_7$.[113–115] According to these redefined rules, since $r_{Y^{3+}}/r_{Zr^{4+}}=1.415$, the δ phase should be the preferred structure and not $Y_2Zr_2O_7$ pyrochlore as proposed by Fan.[113] $Ho_2Hf_2O_7$ and $Ho_2Zr_2O_7$ have been similarly controversial.[116–118] According to our updated ratio-radius rules, $Ho_2Hf_2O_7$ is exactly between the pyrochlore and δ phase while $Ho_2Zr_2O_7$ is more likely to be δ phase than pyrochlore. Finally, when $r_{A^{3+}}/r_{B^{4+}}$ is less than 1.21, a disordered fluorite is the most stable. In summary, the $r_{A^{3+}}/r_{B^{4+}}$ radius-ratio limits are as follows: disordered fluorite $<1.21<\delta$ phase $<1.42-1.44<$ pyrochlore $<1.78-1.83<$ monoclinic pyrochlore <1.92.

We can use these updated rules to predict structures for which no experimental data exists. For example, $r_{In^{3+}}/r_{Ti^{4+}}=1.52$ and $r_{In^{3+}}/r_{Ru^{4+}}=1.48$. Both of these compounds should form $A_2B_2O_7$ pyrochlores, i.e., $In_2Ti_2O_7$ and $In_2Ru_2O_7$, respectively. On the other hand, $r_{In^{3+}}/r_{Mo^{4+}}=1.415$, which is on the cusp between pyrochlore and δ phase (and identical to the radius ratio for Y^{3+} and Zr^{4+}, see above), and therefore more difficult to predict. Other heretofore unobserved structures include $Sc_4Ru_3O_{12}$, $Sc_4Mo_3O_{12}$, $In_4Hf_3O_{12}$, and $In_4Zr_3O_{12}$. According to our radius-ratio rules, these should all form δ-phase structures. In the following sections we describe in detail the predicted structure of these compounds.

B. Structural analysis of ideal δ-phase compounds

Three unique cation structures for ordered δ-phase compounds were identified by the CEMMC method. In order to compare the differences between these similar structures, it is instructive to consider the ideal (i.e., unrelaxed) structures of these three configurations according to their layer motifs.[119] The layer motif perspective is a useful way to visualize the structure of complex ceramics, where, in the example of a cubic structure, {111}-type planes are stacked along $\langle 111\rangle$ axes with $\bar{3}$ symmetry. The ideal unit cell for δ phase (using a hexagonal description) incorporates three $A_4B_3O_{12}$ molecules in an atomic arrangement that closely resembles fluorite (CaF_2). Thus, there are 21 A^{3+} and B^{4+} metal cations (collectively denoted in this section as M) and 36 oxygen anions (denoted as O) per unit cell. Perhaps the simplest way to visualize the δ-phase crystal structure is as a set of layers stacked along the c axis of the unit cell. In Fig. 2, a representative δ-phase configuration (δ_1) is shown edge on. Viewed in this way, it is convenient to consider the δ-phase unit cell as consisting of three trilayer slabs. Each trilayer slab is comprised of a central M layer with O layers above and below. Thus, the trilayer slab can be denoted as O-M-O. Furthermore, each trilayer slab contains one M_7O_{12} molecular unit per unit cell, and therefore, three trilayer slabs makes three molecular units of $A_4B_3O_{12}$ per unit cell. It should be noted that in Fig. 2, the c component of the lattice parameter has been artificially doubled with respect to the actual c in order to better distinguish the O-M-O trilayer slabs. The differences between δ-phase configurations are the ways in which the cations are arranged within the M layers.

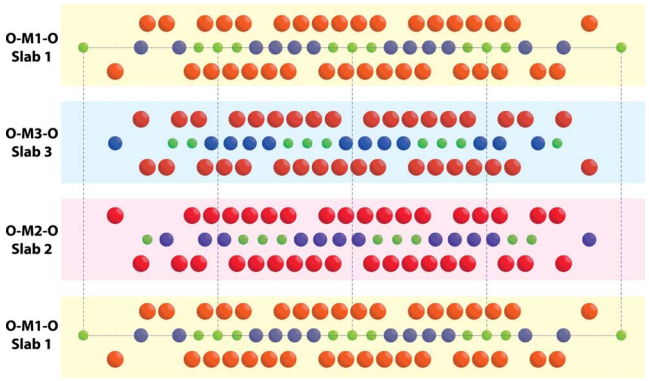

FIG. 2. (Color online) Representative layering sequences of cations and anions for the δ-phase structure, where red atoms are oxygen, blue atoms are A^{3+} cations, and green atoms are B^{4+} cations. For simplicity, only the δ_1 structure is shown.

Clearly the $A:B$ ratio in a unit cell of δ phase must equal 4:3. However, the number of A and B cations in each O-M-O slab can vary so long as the 4:3 ratio is achieved by the sum of three slabs. Table II describes the four different possible ways that A and B cations can be distributed in the three O-M-O slabs to yield an average $A:B=4:3$ per unit cell. We have limited our consideration to cases where at least two of the layers have the same number of A and B cations. Of course, there are eight more layer configurations possible if all layers are allowed to differ. Nevertheless, in model 1 (as denoted in Table II), each M layer has the same cation stoichiometry, which is equivalent to the molecular ratio of cations (4:3). This is the model that is exhibited by both δ_1 and δ_2 structures.[23,24] The difference between model 1 and the

TABLE II. Various possible distributions of A and B cations in the three M layers per δ-$A_4B_3O_{12}$ unit cell, where "slab number" refers to an O-M-O trilayer along the c axis. The δ_1 and δ_2 structures utilize model 1 while δ_3 utilizes model 2.

Model number	Slab number	A cations	B cations
1	3	4	3
	2	4	3
	1	4	3
	Σ	12	9
2	3	6	1
	2	3	4
	1	3	4
	Σ	12	9
3	3	2	5
	2	5	2
	1	5	2
	Σ	12	9
4	3	0	7
	2	6	1
	1	6	1
	Σ	12	9

remaining models is that in models 2–4, none of the slabs exhibit an $A:B$ cation ratio of 4:3, and slab 3 is different from slabs 1 and 2 (which are the same). Models 2–4 yield a "block" structure along the c axis. The δ_3 structure utilizes the block structure shown in model 2. Models 3 and 4 were not identified in any of the low-energy structures found in this study.

Revisiting Fig. 2, we recall that there are nine atomic layers along the c axis per δ unit cell—three pure M layers and six pure O layers. There are seven M cations and six O anions per layer per unit cell. Each M layer consists of a "fully dense" triangular net of M atoms[119] while a periodic series of missing oxygen atoms results in the O layers being 6/7 dense (with respect to the M layers). The vacancy pattern in each O layer is analogous to the surface-atom pattern in the so-called 7×7 reconstruction of the (111) surface of Si.[120–122] The remaining 6/7 dense atom pattern is a $3^4.6$ Archimedean tiling, which is defined as a motif where five polygons meet at a vertex, four of which are triangles and one of which is a hexagon (hence $3^4.6$).[123] This structure is the same for all oxygen layers in all δ-phase compositions (only the registry is shifted). Figure 3 shows this oxygen layer structure and also highlights the $3^4.6$ Archimedean-tiling pattern.

The plan view of the layer patterns for A and B cations in M layers is shown in Figs. 4(a)–4(c) for δ_1, δ_2, and δ_3, respectively. Each layer diagram depicts a section extending 2×2 unit cells. The three M layers in δ_1 are identical except for lateral registry shifts of the layers. The same is true for the δ_2 structure. The difference between δ_1 and δ_2 is how the cations are arranged within the M layers. In both structures there are seven M atoms per layer per unit cell, and as discussed above, the stoichiometric ratio 4:3 is maintained in each layer. However, the cations in δ_1 are arranged in herringbone lines along the $\langle110\rangle$ direction while in δ_2, the main feature is the equilateral triangles of B^{4+} (small green) atoms surrounded on all sides by A^{3+} (large blue) cations. Also, in δ_1, the $3a$ sixfold sites are exclusively occupied by B^{4+} cations while in δ_2 the $3a$ sites are exclusively occupied by A^{3+} cations. The δ_3 structure is rather different and has not been reported before in the literature; although, as with the δ_1 structure, the $3a$ sites in δ_3 are exclusively occupied by B^{4+} cations. The difference between δ_1 and δ_3 is the configuration of cations on $18f$ sites. In δ_3, the M1 and M2 layers are identical except for a registry shift. However the $A:B$ cation ratio in these layers is 3:4 (as opposed to stoichiometric 4:3). Therefore, in order to preserve stoichiometry in the unit cell, the M3 layer must have an $A:B$ ratio of 6:1 (see model 2 in Table II). The topological feature of the δ_3-phase cation structure is that layers M1 and M2 consist of equilateral triangles of A^{3+} and B^{4+} cations while the M3 layer has B^{4+} atoms surrounded on all sides by A^{3+} cations; again a $3^4.6$ Archimedean tiling.

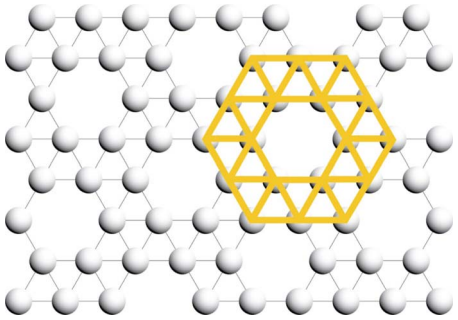

FIG. 3. (Color online) The structure of the oxygen layers in δ phase, where the $3^4.6$ Archimedean-tiling pattern is highlighted.

Finally, the O layers surrounding each M layer in the O-M-O slabs lead to differences in the anion nearest-neighbor (nn) coordination number around each cation. Within each M layer, six cations (per M layer per unit cell) are sevenfold-coordinated by n.n. O anions ($18f$ site) while the seventh cation is sixfold coordinated by nn O anions ($3a$ site). The sixfold-coordinated cation sites are denoted in Fig. 4 by small hexagons around the cations residing on $3a$ sites. A distinguishing difference between the δ_1 and δ_2 structures is evident in Figs. 4(a) and 4(b), respectively, namely, that the sixfold $3a$ cation sites in δ_1 [Fig. 4(a)] are occupied by B^{4+} atoms while in δ_2 [Fig. 4(b)], these sites are occupied by A^{3+} atoms. Since smaller coordination numbers tend to favor smaller cations, the δ_1 structure seems more likely, based on this criterion alone. In the δ_3 structure [Fig. 4(c)], the sixfold $3a$ cation sites are occupied exclusively by B^{4+} atoms, as in the δ_1 structure. The implications of these differences in coordination between the structures will be discussed in the following section.

C. Cation ordering of relaxed δ-phase compounds

Table III compares the energy calculated with DFT for δ_1, δ_2, and δ_3 of delta-phase compounds in ascending order of $r_{A^{3+}}/r_{B^{4+}}$, where the eightfold and sixfold coordinations of

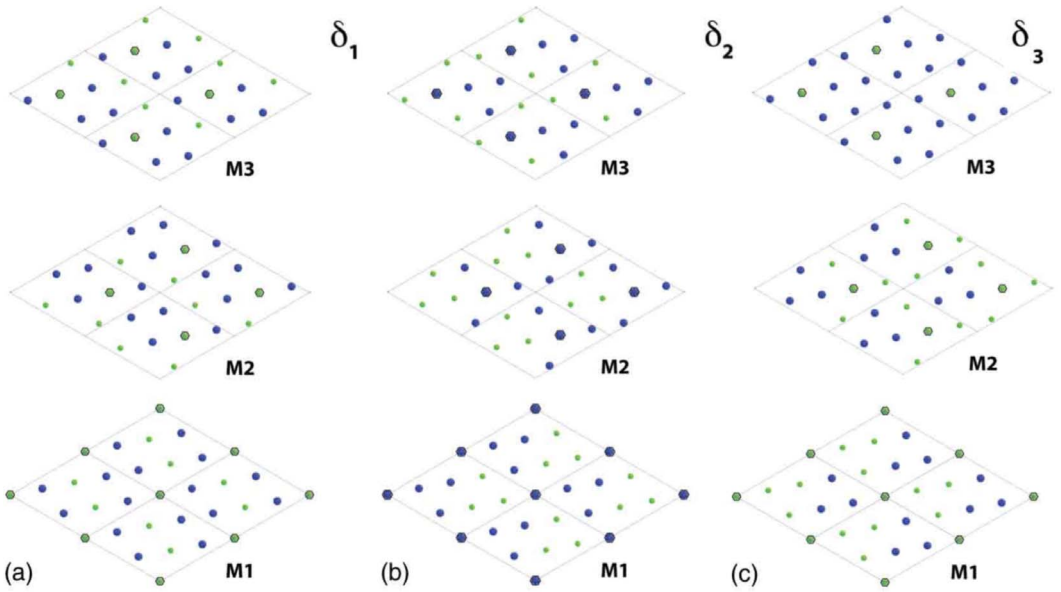

FIG. 4. (Color online) Plan view of the three cation layers of δ_1, δ_2, and δ_3 phases.

A^{3+} and B^{4+} radii are used, respectively. For each composition, energies are presented relative to the disordered configuration (where "disordered" in this case only refers to 18*f* cations and was determined using SQS), and the lowest-energy structure for a particular compound is denoted by italics. First, we notice that for each composition, there is an ordered cation arrangement for which the energy is negative. This means that the thermodynamic ground state is an ordered structure and not random; although, for a few compounds such as $Sc_4Hf_3O_{12}$ and $Sc_4Mo_3O_{12}$, the ordered energy is only slightly preferred over random. Second, we observe that the δ_1 structure is the lowest-energy structure for most of the compounds considered (12 of 17). Additionally, and in agreement with Bogicevic *et al.*,[23] we found the δ_1 structure to be the ground state for $Y_4Zr_3O_{12}$. Also in agreement with Bogicevic *et al.*,[24] we found the ground state of $Sc_4Zr_3O_{12}$ to be the δ_2 structure. We also found this structure to be the ground state of $In_4Zr_3O_{12}$ and $In_4Hf_3O_{12}$. Although there is a slight preference of the δ_3 structure for $Sc_4Hf_3O_{12}$, the δ_1, δ_2, and δ_3 structures are essentially degenerate. In fact, only one composition strongly prefers the δ_3 structure, $Sc_4Ru_3O_{12}$.

Next, we observe that the energy difference between the lowest-ordered structure and random for all compounds is

TABLE III. Lattice energies calculated with respect to random (in eV per $A_4B_3O_{12}$ formula unit) for three ordered δ-phase structures. Order-disorder temperatures (T_{OD}), determined by DFT, for the ground-state structure are also provided. The compositions are ordered according their respective $r_{A^{3+}}/r_{B^{4+}}$ cation radius ratios where the A^{3+} cation is eightfold coordinated and the B^{4+} cation is sixfold coordinated. More accurate radius ratios reflecting the actual coordination of the cations are also provided for the three δ-phase structures in the last two columns.

Composition	r_A/r_B (VIII/VI)	δ_1 (eV)	δ_2 (eV)	δ_3 (eV)	T_{OD} (K)	r_A/r_B (δ_1 and δ_3)	r_A/r_B (δ_2)
$Sc_4Zr_3O_{12}$	1.21	−0.087	−0.237	−0.087	718	1.06	1.02
$Sc_4Sn_3O_{12}$	1.26	−0.156	0.466	−0.004	474	1.11	1.06
$In_4Zr_3O_{12}$	1.28	0.052	−0.295	−0.090	894	1.13	1.08
$In_4Sn_3O_{12}$	1.33	−0.199	0.437	−0.120	603	1.18	1.13
$Sc_4Mo_3O_{12}$	1.34	−0.084	0.425	0.380	255		
$Lu_4Zr_3O_{12}$	1.36	−0.142	0.100	−0.027	432	1.21	1.16
$Er_4Zr_3O_{12}$	1.39	−0.183	0.289	−0.012	556	1.24	1.19
$Sc_4Ru_3O_{12}$	1.40	0.147	0.677	−0.402	1219		
$Ho_4Zr_3O_{12}$	1.41	−0.197	0.348	−0.009	597	1.26	1.21
$Y_4Zr_3O_{12}$	1.42	−0.217	0.412	−0.007	658	1.26	1.21
$Lu_4Sn_3O_{12}$	1.42	−0.271	1.012	−0.022	821	1.26	1.21
$Sc_4Ti_3O_{12}$	1.44	−0.314	0.682	−0.020	951	1.24	1.18

TABLE IV. Sevenfold ionic radii, calculated from the sixfold and eightfold radii of Shannon (Ref. 14).

Cation	Sevenfold radius (Å)
Ti^{4+}	0.6725
Sc^{3+}	0.8075
In^{3+}	0.860
Lu^{3+}	0.919
Ho^{3+}	0.958

relatively small; that is, the thermodynamic driving force to form an ordered phase is small. Consequently, as can be seen in Table III, the order-disorder temperatures are quite low, suggesting that very long annealing times at temperatures just below the order-disorder temperature (T_{OD}) would be necessary to form a completely ordered phase. Values for T_{OD} were calculated using the following equation:

$$T_{OD} \approx \frac{\Delta E_{disorder}}{\Delta S_{ideal}}, \tag{3}$$

where $\Delta E_{disorder}$ is the calculated disorder energy and ΔS_{ideal} is the ideal configurational entropy (and the effects of vibrational entropy are neglected).

We also observe that there is no clear trend in the cation-ordering tendencies as a function of $r_{A^{3+}}/r_{B^{4+}}$. Indeed, it has previously been proposed,[21] and intuition would lead one to expect, that δ-phase compounds with similar A^{3+} and B^{4+} cation radii are more likely to exhibit cation disorder. According to Table III, this does not seem to be the case. However, as described in the previous section, the eightfold and sixfold radii for A^{3+} and B^{4+} are not the actual coordinations of these cations (although they are still useful in illustrating the structure vs composition trends in Fig. 1). Rather, in the δ-phase structure, cations can be either sixfold or sevenfold coordinated, and the number of A^{3+} and B^{4+} cations per unit cell that are sixfold or sevenfold coordinated depends upon the particular δ-phase structure in question. For example, all A^{3+} cations in both δ_1 and δ_3 are sevenfold coordinated while 1/3 of the B^{4+} cations are sixfold coordinated and the remaining 2/3 are sevenfold coordinated. In the δ_2 structure, all of B^{4+} cations are sevenfold coordinated while 1/4 of A^{3+} cations are sixfold coordinated and the remaining 3/4 are sevenfold coordinated. For this reason, it is worthwhile to reconsider the energies of the three δ-phase structures in terms of more accurate B cation ratios.

Unfortunately, Shannon[14] only provided sevenfold ionic radii for Er^{3+}, Y^{3+}, Sn^{4+}, Hf^{4+}, and Zr^{4+}. Since the sevenfold radii that Shannon does provide turn out to be simple averages of sixfold and eightfold radii, we have calculated sevenfold radii in a similar fashion for cations where sixfold and eightfold radii (but not sevenfold) are reported by Shannon (see Table IV). Eightfold radii do not exist for Mo^{4+} and Ru^{4+}, thus we were not able to generate sevenfold radii for these cations. Nevertheless, we used sevenfold cationic radii for all δ-phase compositions without Mo^{4+} or Ru^{4+}, to generate $r_{A^{3+}}/r_{B^{4+}}$ values that explicitly consider the appropriate coordination of A^{3+} and B^{4+} cations. These ratios are given in the last two columns of Table III for the three δ-phase structures considered (δ_1 and δ_3 have the same cation coordination). It is interesting to note that for $Sc_4Zr_3O_{12}$ and $Sc_4Hf_3O_{12}$, $r_{A^{3+}}/r_{B^{4+}}$ is nearly 1 for δ_1 and δ_3, and even closer to 1 for δ_2. The preference of the δ_2 structure for compounds with similar A and B cationic radii, e.g., $Sc_4Zr_3O_{12}$ (recall the three δ-phase structures for $Sc_4Hf_3O_{12}$ are degenerate) presents an interesting competition between the Pauling and Verwey-Heilmann concepts of ionic coordination. Recall Pauling's structural rules of ionic bonding state that smaller cations prefer lower coordination.[108,124] Verwey and Heilmann[125] rather propose that cations of high valence will have large coordination numbers. The Verwey-Heilmann rule appears to be obeyed by the δ_2 structure, where all 4+ cations are sevenfold coordinated (on 18f sites) while the 1/4 of 3+ cations are sixfold coordinated (on 3a sites) and 3/4 are sevenfold coordinated. However, the δ_2 structure also roughly obeys Pauling's rule since for the δ_2 structure, the A^{3+} and B^{4+} cation radii are very similar (which is clearly not the case if the eightfold and sixfold radii of A^{3+} and B^{4+} are considered). A similar competition between these two coordination principles has been observed for spinels.[126] However, for the δ_1 and δ_3 structures, this struggle between coordination principles is not as pronounced. That is, both δ_1 and δ_3 structures violate the Verwey-Heilmann principle with the higher valence cation (B^{4+}) preferentially occupying the less coordinated site (sixfold 3a). Furthermore, for all compositions where the A^{3+} cation radius is appreciably larger than the B^{4+} cation radius, the δ_1 and δ_3 structures are preferred over the δ_2 structure. In these cases, it appears as though the δ_1 and δ_3 structures obey Pauling's rule, with the smaller B^{4+} cation exclusively occupying the lower coordinated, sixfold 3a site.

In addition to having the most similarly sized A and B cations, $Sc_4Zr_3O_{12}$ and $Sc_4Hf_3O_{12}$ are also noteworthy in that all three ordered δ-phase structures are lower energy than the random structure, which is unique to all compounds considered in this study. Therefore, that fully ordered $Sc_4Zr_3O_{12}$ and $Sc_4Hf_3O_{12}$ δ phases have not been observed experimentally may be in part to the low T_{OD} but also due to the relative preference for multiple ordered structures over random.

Trends exist within compositions with similar B^{4+} cations. For example, the preference of the δ_2 structure increases for $A_4Zr_3O_{12}$ compounds with increasing $r_{A^{3+}}/r_{Zr^{4+}}$ until $Lu_4Zr_3O_{12}$, when δ_1 is preferred ($Y_4Zr_3O_{12}$ only slightly strays from this trend). As $r_{A^{3+}}/r_{Zr^{4+}}$ increases from $Lu_4Zr_3O_{12}$, the preference for the δ_1 structure increases. A similar trend is observed for the $A_4Hf_3O_{12}$ series. Again the trend is evident for $A_4Sn_3O_{12}$ compositions, although the δ_2 structure is never preferred. Since there is only one $A_4Ti_3O_{12}$ compound ($Sc_4Ti_3O_{12}$), it is not possible to determine a trend. Finally, presumably due to the open electronic structure of Ru and Mo and their ability to exhibit multiple valence states, $Sc_4Mo_3O_{12}$ and $Sc_4Ru_3O_{12}$ behave differently than the other δ-phase compounds.

The structural details of all compositions considered are provided for the ground-state structure in Table V. For all compositions where δ_1 is the ground-state structure, $a \neq b$.

TABLE V. DFT predicted structural properties of δ phases in their ground-state structures.

Compound	Ground-state structure	a	b	c	α	β	γ	Band gap (eV)
$Sc_4Zr_3O_{12}$	δ_2	9.48	9.48	8.78	90°	90°	120°	4.15
$Sc_4Sn_3O_{12}$	δ_1	9.55	9.50	8.81	89.2°	91.6°	121.1°	2.97
$In_4Zr_3O_{12}$	δ_2	9.71	9.71	8.92	90°	90°	120°	2.83
$In_4Sn_3O_{12}$	δ_1	9.73	9.67	9.00	88.8°	91.9°	121.0°	1.06
$Sc_4Mo_3O_{12}$	δ_1	9.41	9.50	8.66	89.2°	91.9°	122.3°	0
$Lu_4Zr_3O_{12}$	δ_1	9.77	9.71	9.05	89.0°	91.2°	120.7°	4.33
$Er_4Zr_3O_{12}$	δ_1	9.89	9.78	9.14	88.6°	91.6°	120.8°	4.30
$Sc_4Ru_3O_{12}$	δ_3	9.25	9.25	8.64	90°	90°	120°	0
$Ho_4Zr_3O_{12}$	δ_1	9.93	9.80	9.18	88.4°	91.8°	120.9°	4.30
$Y_4Zr_3O_{12}$	δ_1	9.99	9.85	9.23	88.3°	91.9°	120.9°	4.22
$Lu_4Sn_3O_{12}$	δ_1	9.86	9.64	9.01	88.1°	92.5°	121.3°	2.71
$Sc_4Ti_3O_{12}$	δ_1	9.36	9.19	8.58	88.0°	92.6°	121.8°	2.94

This is in contrast to the δ_2 and δ_3, where for all cases $a=b$. For compounds where $a \neq b$ (i.e., δ_1), an average of a and b was used to calculate c/a. Hexagonal unit-cell volumes were calculated by $\frac{\sqrt{3}}{2}abc$.

In addition to cation radius, we have also used the c/a structural parameter to discern possible trends in δ-phase cation configurations. Figure 5 compares the calculated c/a values for the lowest-energy ordered and disordered structures (on the abscissa) to the available experimental data (on the ordinate). The ideal value for δ phase c/a [$\sqrt{6/7}$ (Ref. 119)] is also indicated in Fig. 5, which both ordered and disodered c/a values for $Sc_4Zr_3O_{12}$ are nearest to. It is interesting to note that the experimental data agrees well with the calculated values for the disordered structures but less well with the lowest-energy ordered structures. For all compositions considered, the c/a value for the ordered structure is lower than either the disordered or the experimentally observed values. Figure 5 may be useful in future experimental searches for ordered δ-phase structures. The agreement between the disordered and experimental c/a values also gives us confidence that the SQS used to describe the disordered state is a reasonable representation of the experimental structure.

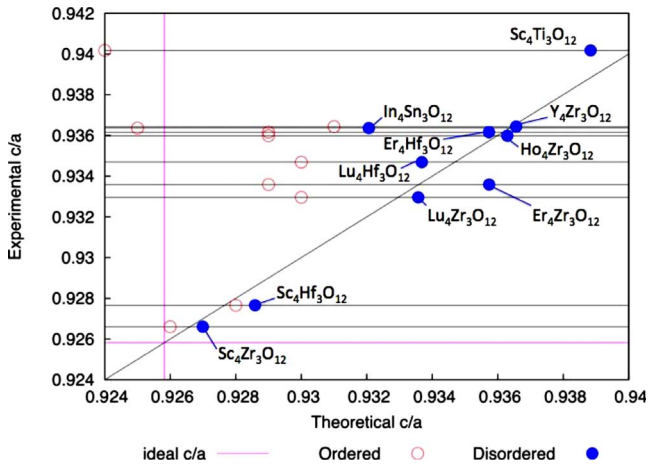

FIG. 5. (Color online) Comparison of experimental to theoretical c/a values for δ-phase compounds (where a is the average of a and b in Table V). Solid circles correspond to values for disordered structures and hollow circles correspond to the lowest-energy ordered structure. Horizontal lines denote specific compounds; along each horizontal line appears an ordered and disordered c/a value for that compound. Also shown are the ideal c/a ($=\sqrt{6/7}=0.9258$) and the slope=1, denoting perfect agreement between theory and experiment.

IV. CONCLUSIONS

We have used a combination of pair-potential Monte Carlo simulations with DFT to predict ordered cation structures for a range of δ-phase compounds. Each of the compositions considered is predicted to exhibit one of three ordered structures identified in this study. Intuition suggests that cation disorder should be more strongly preferred in δ-phase compounds where the cation radii are similar. On the contrary, we observe that the subtleties of cation ordering appear to be governed by electronic effects. For example, we predict that $Sc_4Mo_3O_{12}$, a compound for which the ionic radii are relatively dissimilar, is the δ-phase compound most likely to exhibit cationic disorder. On the other hand, $Sc_4Zr_3O_{12}$, the δ-phase compound for which the cationic radii are most similar is predicted to order more readily than many of the compositions considered. Nevertheless, the difference in energy between "random" (not accounting for anion disorder) and ordered phases is generally small for all δ-phase compositions. In $A_2B_2O_7$ pyrochlores, we have observed a relationship between the calculated order-disorder energy difference and amorphization resistance (e.g., the energy difference between ordered and disordered $A_2Ti_2O_7$ is relatively large and these compounds readily amorphize, see Refs. 8, 13, and 127). If oxygen disorder contributes to the overall disorder of all δ-phase compounds in ways similar to pyrochlore, it might be that this entire class of compounds is amorphization resistant. This will be the topic of a future paper.

Additionally we have generated an ABO_{4-x} structure—composition map that can be used to identify the structure of

compositions ranging from Sc^{3+} to La^{3+} for A^{3+} and Ti^{4+} to Ce^{4+} for B^{4+}. From this structure map, we have predicted the structure of compounds not yet reported in the literature: $In_2Ti_2O_7$ and $In_2Ru_2O_7$ are predicted to be pyrochlores, and $Sc_4Ru_3O_{12}$, $Sc_4Mo_3O_{12}$, $In_4Hf_3O_{12}$, and $In_4Zr_3O_{12}$ are predicted to be δ phase. Furthermore, we have explained the structure of the three δ phases discussed in detail using the layer motif method. Finally, we have interpreted our results of δ-phase preference in terms of cationic radius ratio and c/a structural arguments. These structural observations of δ-phase compositions can be used to interpret trends in materials properties such as radiation tolerance.

ACKNOWLEDGMENTS

This work was sponsored by the U.S. Department of Energy, Office of Basic Energy Sciences, Division of Materials Science and Engineering, and carried out in part for the UKERC materials programme. Los Alamos National Laboratory, an affirmative action/equal opportunity employer, is operated by Los Alamos National Security, LLC, for the National Nuclear Security Administration of the U.S. Department of Energy under Contract No. DE-AC52-06NA25396.

*stanek@lanl.gov

[1] D. R. Clarke and S. R. Phillpot, Mater. Today **8**, 22 (2005).
[2] H. L. Tuller, Solid State Ion. **52**, 135 (1992).
[3] B. C. H. Steele, Solid State Ionics **12**, 391 (1984).
[4] N. P. Brandon, S. Skinner, and B. C. H. Steele, Annu. Rev. Mater. Res. **33**, 183 (2003).
[5] *Uranium Dioxide: Properties and Nuclear Applications*, edited by J. Belle (U.S. Atomic Energy Commission, Washington, D. C., 1961).
[6] C. R. Stanek, J. A. Valdez, K. E. Sickafus, K. J. McClellan, and R. W. Grimes, Ceram. Eng. Sci. Proc. **27**, 11 (2007).
[7] W. J. Weber, R. C. Ewing, C. R. A. Catlow, T. Diaz de la Rubia, L. W. Hobbs, C. Kinoshita, Hj. Matzke, A. T. Motta, M. Nastasi, E. K. H. Salje, E. R. Vance, and S. J. Zinkle, J. Mater. Res. **13**, 1434 (1998).
[8] K. E. Sickafus, L. Minervini, R. W. Grimes, J. A. Valdez, M. Ishimaru, F. Li, K. J. McClellan, and T. Hartmann, Science **289**, 748 (2000).
[9] S. X. Wang, B. D. Begg, L. M. Wang, R. C. Ewing, W. J. Weber, and K. V. Govdan Kutty, J. Mater. Res. **14**, 4470 (1999).
[10] K. E. Sickafus, Hj. Matzke, T. Hartmann, K. Yasuda, J. A. Valdez, P. Chodak III, M. Nastasi, and R. A. Verrall, J. Nucl. Mater. **274**, 66 (1999).
[11] N. S. Kunakov, Z. Anorg. Chem. **52**, 430 (1907).
[12] L. Minervini, R. W. Grimes, and K. E. Sickafus, J. Am. Ceram. Soc. **83**, 1873 (2000).
[13] K. E. Sickafus, R. W. Grimes, J. A. Valdez, A. R. Cleave, M. Tang, M. Ishimaru, S. M. Corish, C. R. Stanek, and B. P. Uberuaga, Nature Mater. **6**, 217 (2007).
[14] R. D. Shannon, Acta Crystallogr., Sect. A: Cryst. Phys., Diffr., Theor. Gen. Crystallogr. **32**, 751 (1976).
[15] V. P. Red'ko and L. M. Lopato, Inorg. Mater. **27**, 1905 (1991).
[16] S. P. Ray, V. S. Stubican, and D. E. Cox, Mater. Res. Bull. **15**, 1419 (1980).
[17] H. Scott, Acta Crystallogr., Sect. B: Struct. Crystallogr. Cryst. Chem. **33**, 281 (1977).
[18] M. R. Thornber and D. J. M. Bevan, J. Solid State Chem. **1**, 536 (1970).
[19] H. J. Rossell, J. Solid State Chem. **19**, 103 (1976).
[20] M. R. Thornber, D. J. M. Bevan, and J. Graham, Acta Crystallogr., Sect. B: Struct. Crystallogr. Cryst. Chem. **24**, 1183 (1968).
[21] N. Nadaud, N. Lequeux, M. Nanot, J. Jové, and T. Roisnel, J. Solid State Chem. **135**, 140 (1998).
[22] L. M. Lopato, V. P. Red'ko, G. I. Gerasimyuk, and A. V. Shevchenko, Inorg. Mater. **27**, 1718 (1991).
[23] A. Bogicevic, C. Wolverton, G. M. Crosbie, and E. B. Stechel, Phys. Rev. B **64**, 014106 (2001).
[24] A. Bogicevic and C. Wolverton, Phys. Rev. B **67**, 024106 (2003).
[25] Y. Yourdshahyan, C. Ruberto, M. Halvarsson, L. Bengtsson, V. Langer, B. I. Lundqvist, S. Ruppi, and U. Rolander, J. Am. Ceram. Soc. **82**, 1365 (1999).
[26] A. Predith, G. Ceder, C. Wolverton, K. Persson, and T. Mueller, Phys. Rev. B **77**, 144104 (2008).
[27] A. Zunger, S. H. Wei, L. G. Ferreira, and J. E. Bernard, Phys. Rev. Lett. **65**, 353 (1990).
[28] S. H. Wei, L. G. Ferreira, J. E. Bernard, and A. Zunger, Phys. Rev. B **42**, 9622 (1990).
[29] C. Jiang, C. Wolverton, J. Sofo, L. Q. Chen, and Z. K. Liu, Phys. Rev. B **69**, 214202 (2004).
[30] M. Born, *Atomtheorie des Festen Zustandes* (Teubner, Leipzig, 1923).
[31] P. P. Ewald, Ann. Phys. (Leipzig) **64**, 253 (1921).
[32] R. A. Buckingham, Proc. R. Soc. London, Ser. A **168**, 264 (1938).
[33] C. R. A. Catlow and W. C. Mackrodt, *Computer Simulation of Solids*, (Springer-Verlag, Berlin, 1982).
[34] M. O. Zacate and R. W. Grimes, Philos. Mag. A **80**, 797 (2000).
[35] M. O. Zacate and R. W. Grimes, J. Phys. Chem. Solids **63**, 675 (2002).
[36] J. A. Ball, M. Pirzada, R. W. Grimes, M. O. Zacate, D. W. Price, and B. P. Uberuaga, J. Phys.: Condens. Matter **17**, 7621 (2005).
[37] N. Metropolis, A. W. Rosenbluth, M. N. Rosenbluth, A. H. Teller, and E. Teller, J. Chem. Phys. **21**, 1087 (1953).
[38] G. Kresse and D. Joubert, Phys. Rev. B **59**, 1758 (1999).
[39] J. P. Perdew, K. Burke, and M. Ernzerhof, Phys. Rev. Lett. **77**, 3865 (1996).
[40] G. Kresse and J. Hafner, Phys. Rev. B **47**, 558 (1993).
[41] G. Kresse and J. Hafner, Phys. Rev. B **49**, 14251 (1994).
[42] G. Kresse and J. Furthmüller, Comput. Mater. Sci. **6**, 15 (1996a).
[43] G. Kresse and J. Furthmüller, Phys. Rev. B **54**, 11169 (1996).
[44] A. V. Prokofiev, A. I. Shelykh, and B. T. Melekh, J. Alloys Compd. **242**, 41 (1996).
[45] N. Hirosaki, S. Ogata, and C. Kocer, J. Alloys Compd. **351**, 31 (2003).

[46] O. Muller and R. Roy, *The Major Ternary Structural Families, Crystal Chemistry of Non-metallic Materials* (Springer, Berlin, 1974).
[47] M. Gasperin, Acta Crystallogr., Sect. B: Struct. Crystallogr. Cryst. Chem. **31**, 2129 (1975).
[48] E. J. Harvey, K. R. Whittle, G. R. Lumpkin, R. I. Smith, and S. A. T. Redfern, J. Solid State Chem. **178**, 800 (2005).
[49] K. Scheunemann and H. Müller-Buschbaum, J. Inorg. Nucl. Chem. **37**, 2261 (1975).
[50] P. A. Koz'min, N. A. Zakharov, and M. D. Surazhskaya, Inorg. Mater. **33**, 850 (1997).
[51] G. Bocquillon, F. Queyroux, Ch. Susse, and R. Collongues, Compt. Rendu. **272C**, 572 (1971).
[52] F. Queyroux, M. Huber, and R. Collongues, Compt. Rendu. **270C**, 806 (1970).
[53] F. Brisse and O. Knop, Can. J. Chem. **46**, 859 (1968).
[54] M. A. Subramanian, G. Aravamudan, and G. V. Subba Rao, Prog. Solid State Chem. **15**, 55 (1983).
[55] O. Knop, F. Brisse, L. Castelli, and R. Sutarno, Can. J. Chem. **43**, 2812 (1965).
[56] H.-J. Deiseroth and H. Müller-Buschbaum, Z. Anorg. Allg. Chem. **375**, 152 (1970).
[57] M. Faucher and P. Caro, J. Solid State Chem. **12**, 1 (1975).
[58] M. P. van Dijk, J. H. H. ter Maat, G. Roelofs, H. Bosch, G. M. H. van de Velde, P. J. Gellings, and A. Burggraaf, Mater. Res. Bull. **19**, 1149 (1984).
[59] T. Yamamoto, R. Kanno, Y. Takeda, O. Yamamoto, Y. Kawamoto, and M. Takano, J. Solid State Chem. **109**, 372 (1994).
[60] H. Kobayashi, R. Kanno, Y. Kawamoto, T. Kamiyama, F. Izumi, and A. Sleight, J. Solid State Chem. **114**, 15 (1995).
[61] B. J. Kennedy, B. A. Hunter, and C. J. Howard, J. Solid State Chem. **130**, 58 (1997).
[62] B. J. Kennedy and T. Vogt, J. Solid State Chem. **126**, 261 (1996).
[63] E. Chtoun, L. Hanebali, P. Garnier, and J. M. Kiat, Eur. J. Solid State Inorg. Chem. **34**, 553 (1997).
[64] M. Field, B. J. Kennedy, and B. A. Hunter, J. Solid State Chem. **151**, 25 (2000).
[65] E. H. Chtoun, L. Hanebali, and P. Garnier, Ann. Chim. (Paris) **25**, 381 (2000).
[66] Y. Tabira, R. L. Withers, T. Yamada, and N. Ishizawa, Z. Kristallogr. **216**, 92 (2001).
[67] C. Bansal, H. Kawanaka, H. Bando, and Y. Nishihara, Phys. Rev. B **66**, 052406 (2002).
[68] N. Taira, M. Wakeshima, Y. Hinatsu, A. Tobo, and K. Ohoyama, J. Solid State Chem. **176**, 165 (2003).
[69] Y. Moritomo, Sh. Xu, A. Machida, T. Katsufuji, E. Nishibori, M. Takata, M. Sakata, and S.-W. Cheong, Phys. Rev. B **63**, 144425 (2001).
[70] O. Knop and F. Brisse, Am. Ceram. Soc. Bull. **46**, 881 (1967).
[71] J. L. Waring and S. J. Schneider, Am. Ceram. Soc. Bull. **43**, 263 (1964).
[72] L. H. Brixner, Inorg. Chem. **3**, 1005 (1964a).
[73] N. I. Timofeeva, S. E. Salibekov, and I. V. Romanovich, Inorg. Mater. **7**, 785 (1971).
[74] W.-J. Becker, Z. Naturforsch. A **25**, 642 (1970).
[75] W.-J. Becker and G. Will, Z. Naturforsch. B **24**, 259 (1969).
[76] F. Jona, G. Shirane, and R. Pepinsky, Phys. Rev. **98**, 903 (1955).
[77] F. Bertaut, F. Forrat, and M. C. Montmory, C. R. Hebd. Seances Acad. Sci. **249**, 829 (1959).
[78] R. J. Bouchard and J. L. Gillson, Mater. Res. Bull. **6**, 669 (1971).
[79] W.-J. Becker and G. Will, Z. Kristallogr. **139**, 278 (1970).
[80] C. G. Whinfrey, D. W. Eckhart, and A. Tauber, J. Am. Chem. Soc. **83**, 755 (1961).
[81] K. N. Portnoi, N. I. Timofeeva, C. E. Salibekov, and I. V. Romanovich, Inorg. Mater. **6**, 73 (1970).
[82] F. M. Spiridinov, V. A. Stepanov, L. N. Komissarova, and V. I. Spitsyn, J. Less-Common Met. **14**, 435 (1968).
[83] M. Perez y Jorba, Ann. Chim. (Paris) **7**, 479 (1962).
[84] F. Queyroux, Compt. Rendu. **259**, 1527 (1964).
[85] B. P. Mandal, N. Garg, S. M. Sharma, and A. K. Tyagi, J. Solid State Chem. **179**, 1990 (2006).
[86] S.-W. Han, J. S. Gardner, and C. H. Booth, Phys. Rev. B **69**, 024416 (2004).
[87] V. P. Buntushkin, I. V. Romanovich, and N. I. Timofeeva, Inorg. Mater. **7**, 1456 (1971).
[88] L. N. Komissarova, B. I. Pokrovski, and V. V. Nechaeva, Dokl. Akad. Nauk SSSR **168**, 1076 (1966).
[89] M. R. Thornber, D. J. M. Bevan, and E. Summerville, J. Solid State Chem. **1**, 545 (1970).
[90] J. Lefèvre, Rev. Hautes Temp. Refract. **1**, 229 (1964).
[91] J. Lefèvre, Ann. Chim. (Paris) **118**, 117 (1963).
[92] G. Brauer and H. Gradinger, Z. Anorg. Allg. Chem. **276**, 209 (1954).
[93] A. Rabenau, Z. Anorg. Allg. Chem. **288**, 221 (1956).
[94] T. Moriga, A. Yoshiasa, F. Kanamaru, K. Koto, M. Yoshimura, and S. Smiya, Solid State Ionics **31**, 319 (1989).
[95] A. W. Sleight, Inorg. Chem. **8**, 1807 (1969).
[96] Ch. K. Jørgensen, R. Papalardo, and E. Rittershaus, Z. Naturforsch. A **20**, 54 (1965).
[97] L. H. Brixner, Inorg. Chem. **3**, 1065 (1964b).
[98] O. Knop, F. Brisse, and L. Castelitz, Can. J. Chem. **47**, 971 (1969).
[99] A. Rouanet, C. R. Hebd. Seances Acad. Sci. **267C**, 1581 (1968).
[100] R. K. Stewart and O. Hunter, J. Am. Ceram. Soc. **53**, 421 (1970).
[101] U. Croatto and A. Mayer, Gazz. Chim. Ital. **73**, 199 (1943).
[102] H. H. Möbius, Z. Chem. **4**, 81 (1964).
[103] H. H. Möbius, H. Witzmann, and F. Zimmer, Z. Chem. **4**, 194 (1964).
[104] J. D. McCullough, J. Am. Chem. Soc. **72**, 1386 (1950).
[105] A. Rouanet, C. R. Hebd. Seances Acad. Sci. **266C**, 1230 (1968).
[106] P. Duwez, F. W. Brown, Jr., and F. Odell, J. Electrochem. Soc. **98**, 356 (1951).
[107] F. Hund, Z. Elektrochem. **55**, 363 (1951).
[108] L. Pauling, *The Nature of the Chemical Bond and the Structure of Molecules and Crystals: An Introduction to Modern Structural Chemistry* (Cornell University Press, Ithaca, NY, 1960).
[109] L. H. Ahrens, Geochim. Cosmochim. Acta **2**, 155 (1952).
[110] D. H. Templeton and C. H. Dauben, J. Am. Chem. Soc. **76**, 5237 (1954).
[111] C. R. Stanek and R. W. Grimes, J. Am. Ceram. Soc. **85**, 2139 (2002).
[112] M. J. D. Rushton, R. W. Grimes, C. R. Stanek, and S. Owens, J. Mater. Res. **19**, 1603 (2004).
[113] F. Fu-K'ang Fan, A. K. Kuznetsov, and E. K. Keler, Izv. Akad. Nauk SSSR, Otd. Khim Nauk **7**, 1141 (1962).
[114] D. K. Smith, J. Am. Ceram. Soc. **49**, 625 (1966).
[115] R. A. Chapman, D. B. Meadowcroft, and A. J. Walkden, J. Phys.

D **3**, 307 (1970).
[116] I. N. Belyaev and S. M. Artamonova, Inorg. Mater. **5**, 76 (1969).
[117] F. M. Spiridinov, Inorg. Mater. **6**, 1222 (1970).
[118] I. N. Belyaev and S. M. Artamonova, Inorg. Mater. **6**, 1224 (1970).
[119] K. E. Sickafus, R. W. Grimes, S. M. Corish, A. R. Cleave, M. Tang, C. R. Stanek, B. P. Uberuaga, and J. A. Valdez, Los Alamos National Laboratory, Technical Report No. LA-14205, 2006 (unpublished).
[120] R. E. Schlier and H. E. Farnsworth, J. Chem. Phys. **30**, 917 (1959).
[121] G. Binnig, H. Rohrer, C. Gerber, and E. Weibel, Phys. Rev. Lett. **50**, 120 (1983).
[122] K. Takayanagi, Y. Tanishiro, S. Takahashi, and M. Takahashi, Surf. Sci. **164**, 367 (1985).
[123] B. Grünbaum and G. Shephard, *Tilings and Patterns* (W.H. Freeman, New York, 1987).
[124] L. Pauling, J. Am. Chem. Soc. **51**, 1010 (1929).
[125] E. J. W. Verwey and E. L. Heilmann, J. Chem. Phys. **15**, 174 (1947).
[126] K. E. Sickafus, J. M. Wills, and N. W. Grimes, J. Am. Ceram. Soc. **82**, 3279 (1999).
[127] C. Jiang, C. R. Stanek, K. E. Sickafus, and B. P. Uberuaga, Phys. Rev. B **79**, 104203 (2009).